Icarus **149**, 222–234 (2001)
doi:10.1006/icar.2000.6477, available online at http://www.idealibrary.com on IDEAL®

Numerical Evaluation of the General Yarkovsky Effect: Effects on Semimajor Axis

Joseph Spitale and Richard Greenberg

Lunar and Planetary Laboratory, University of Arizona, Tucson, Arizona 85721-0092
E-mail: spitale@lpl.arizona.edu

Received January 19, 2000; revised July 3, 2000

The Yarkovsky effect may play a key role in the orbital evolution of asteroids and near-Earth objects. To evaluate the acceleration under a wide range of conditions, a three-dimensional finite-difference solution to the heat equation is applied to homogeneous, spherical stony bodies with 1-, 10-, and 100-m diameters. This approach employs neither the linearized boundary conditions, the plane-parallel heat flow approximation, nor the assumption of fast rotation used in earlier work. Thus we can explore a wide range of orbital elements and physical properties. Our work agrees well with earlier results in the regimes where their approximations are valid. We investigate a wide range of spin states, including both the "seasonal" (very fast rotation) and "diurnal" (zero obliquity) extremes of the Yarkovsky effect. We find that, for orbits with high eccentricity, the semimajor axis can change much faster than for circular orbits. For such orbits, the orientation of the rotation axis with respect to the direction of pericenter is critical in determining the evolution. A stony main-belt asteroid of diameter 1 m on a high-eccentricity orbit could change its semimajor axis by more than 1 AU in 1.5 Myr.

Key Words: **asteroids; dynamics; meteorites; meteoroids.**

1. INTRODUCTION

The Yarkovsky effect is a net radiative reaction force on a rotating body caused by its asymmetric surface temperature distribution. This force can produce substantial changes in the orbital elements of a small body over relatively short timescales. A number of discrepancies in models regarding the delivery of asteroidal material from main-belt orbits to Earth-crossing orbits may potentially be resolved by properly incorporating the Yarkovsky effect. For example, Wetherill (1985, 1987) suggested that material en route to Earth is injected into the strongest resonances by impacts and breakup events. While such direct injection certainly must occur, the major resonances are quite narrow and the injection efficiency is uncertain. The Yarkovsky effect has been suggested as a mechanism by which to drag much more material into the resonances (Peterson 1976; Rubincam 1995; Afonso *et al.* 1995; Farinella and Vokrouhlický 1999; Vokrouhlický and Farinella 2000). Wetherill (1985, 1987) also proposed that the strongest resonances delivered most meteorites to the Earth. Indeed, fireball data (Wetherill and ReVelle 1981; Halliday *et al.* 1996) seem to suggest that small bodies enter the Earth's atmosphere with orbital elements that are consistent with these strong main-belt resonances. However, Farinella *et al.* (1994) and Gladman *et al.* (1997) found that the strong resonances are actually very inefficient at delivering material to the inner Solar System because they pump asteroid eccentricities so quickly that most bodies become Sun-grazers or Jupiter-crossers before being removed from the resonance by a close encounter with a terrestrial planet. In this paper, we suggest that this conundrum might be resolved by considering the Yarkovsky effect on small bodies after their eccentricities have been enhanced by such a resonance.

The Yarkovsky effect has been studied by many authors (Öpik 1951; Radzievskii 1952; Peterson 1976; Rubincam 1995, 1998; Vokrouhlický and Farinella 1998, 1999; Vokrouhlický and Brož 1999; Farinella *et al.* 1998; Farinella and Vokrouhlický 1999). However, due to the various approximations employed by each author, the parameter space accessible to those methods is limited, and the Yarkovsky effect has yet to be thoroughly characterized. Peterson (1976) used a Fourier expansion truncated at fourth order to explore the so-called "diurnal" Yarkovsky effect, caused by rotation. Rubincam (1987, 1988) identified the "seasonal" Yarkovsky effect and studied it (Rubincam 1995, 1998) by linearizing the radiative boundary condition, so his results are only valid for small eccentricities. Vokrouhlický and Farinella (1998) have developed a nonlinearized treatment of the seasonal effect which is valid for large bodies (because of the plane-parallel approximation). Vokrouhlický and Farinella (1999) removed the restriction to large bodies, but that approach is impractical for fairly large eccentricities. In addition, other effects that might be important in determining the surface temperature distribution have not been fully addressed in previous work. These effects include insulation by regoliths (recently modeled by Vokrouhlický and Brož (1999)), nonspherical shapes (addressed in Vokrouhlický and Farinella (1998)), fractures in the rock, and the temperature dependence of thermal conductivity and heat capacity.

In order to address the above problems and to obtain more general solutions, we compute the Yarkovsky force directly by

0019-1035/01 $35.00

numerically solving the heat equation throughout an orbiting body with solar insolation boundary conditions. For a given set of fixed orbital elements, perturbations to the elements are computed by numerically averaging the Gaussian perturbation equations over a single orbit. This calculation addresses the full nonlinear, spherical problem. It is valid, in principle, for any set of orbital elements and for any spin state. It can treat bodies with realistic physical structures and properties.

In this paper, we use our numerical approach to (1) provide an independent test of earlier solutions where those models were valid and (2) extend the theory to regimes which have not been treated. We present the rates of change of semimajor axis in a coarse reconnaissance of the parameter space consisting of semimajor axis, eccentricity, spin axis direction, and size. Subsequent papers will address changes in other elements, as well as bodies with a broader range of structures and physical properties. In Section 2, we briefly describe the fundamental physics of the problem. In Section 3, we describe the computational approach and the model assumptions and limitations. Section 4 presents the results of our survey. Section 5 discusses the implications of these results for the orbital evolution of small bodies in the inner solar system.

2. BACKGROUND

The asymmetric temperature distribution on the surface of a body rotating in the solar radiation field results in a small net force on the body, due to the momentum carried away by the radiated photons. This net force can cause the orbital elements of the body to change in various ways, depending on the geometry of the orbit relative to the rotation axis.

The following symbols are used throughout this paper: a, e, i, and ϖ are the semimajor axis, eccentricity, inclination, and longitude of periapse, respectively, of the asteroid's orbit. α is the angle between the periapse direction and the projection of the asteroid's spin vector on the orbital plane. ι is the obliquity of the asteroid's spin vector, relative to the orbital angular momentum vector. p is the asteroid's rotation period. D is the diameter of the asteroid. **F** is the net Yarkovsky force on the asteroid.

Consider a body on a circular orbit with its rotation axis normal to the orbital plane (Fig. 1). Because of the body's rotation, thermal inertia will cause the surface temperature distribution to be slightly asymmetric relative to the sun. For prograde rotation (Fig. 1a), the transverse force component is in the direction of orbital motion, so a will increase. Similarly, for retrograde rotation (Fig. 1b), a will decrease. For a slightly eccentric orbit, Peterson (1976) showed that e will also increase for prograde rotation and decrease for retrograde rotation, and that ϖ will always regress. This "diurnal" form of the Yarkovsky effect has the greatest effect on a when the obliquity is 0 or π, and no effect on a when $\iota = \pi/2$. Indeed, Öpik (1951) showed that da/dt caused by the diurnal effect varies as $\cos \iota$. Moreover, the diurnal effect turns off when the rotation is so fast that the surface temperature distribution is smeared out with no longitudinal variation.

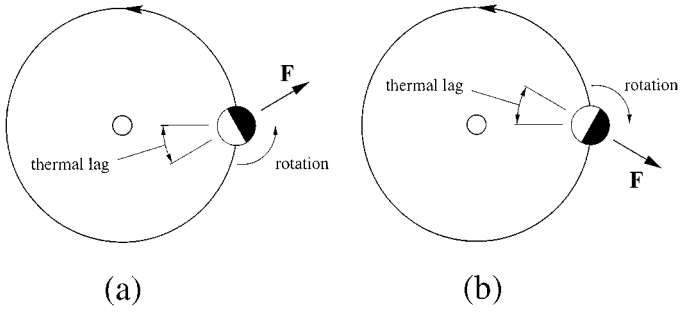

FIG. 1. A body on a circular orbit with its rotation axis normal to the orbital plane. (a) For prograde rotation, the transverse force component is in the same direction as the orbital motion, causing the semimajor axis to increase. (b) For retrograde rotation, the transverse force component is directed opposite to the direction of orbital motion, resulting in semimajor axis decay.

This smearing occurs when a body rotates fast enough that the thermal pulse is unable to penetrate significantly.

When ι is not zero, there is an additional forcing frequency corresponding to the orbital period of the body. Furthermore, when the rotation of the body is very fast, such that the diurnal contribution is negligible, the forcing is purely seasonal. In this "seasonal" case, the Yarkovsky effect has the greatest effect on a when the rotation axis lies in the plane of the orbit ($\iota = \pi/2$) and has no effect on a when $\iota = 0$. Rubincam (1987) showed that da/dt caused by the pure seasonal effect varies as $\sin^2 \iota$.

Figure 2 shows the orientation of the force vector at various points in a circular orbit for a fast-rotating body with $\iota = \pi/2$. In part (a) there is no seasonal lag shown. At positions (1) and (3), when the rotation axis points directly toward or away from the sun, the surface temperature distribution is highly asymmetric, producing a large radial Yarkovsky force vector oriented parallel to the spin axis. At points (2) and (4), when the rotation axis is perpendicular to the radial direction, there is no surface temperature asymmetry to produce a net force vector. There are two quadrants of the orbit (2–3 and 4–1) in which the transverse force component is in the same direction as the orbital motion (producing an instantaneous increase in a) and two quadrants (1–2 and 3–4) in which the transverse force component is directed opposite to the orbital motion (producing an instantaneous decrease in a). With no seasonal thermal inertia, the situation is completely symmetric, so the instantaneous changes in a cancel out over an orbit, resulting in no net change.

In Fig. 2b, the seasonal lag causes each thermal state to occur a bit later in the orbit. Again, there are two quadrants of the orbit (2–3 and 4–1) in which the transverse force produces an instantaneous increase in a and two quadrants (1–2 and 3–4) in which the transverse force produces an instantaneous decrease in a. In this case, however, the larger kicks occur in quadrants 1–2 and 3–4, where the transverse force produces an instantaneous decrease in a. Averaged over an orbit, the forces that increase a do not completely cancel the forces that decrease a, so there is a net decay of the semimajor axis. For this purely seasonal (very fast rotation) case with small eccentricity, Rubincam (1995) showed

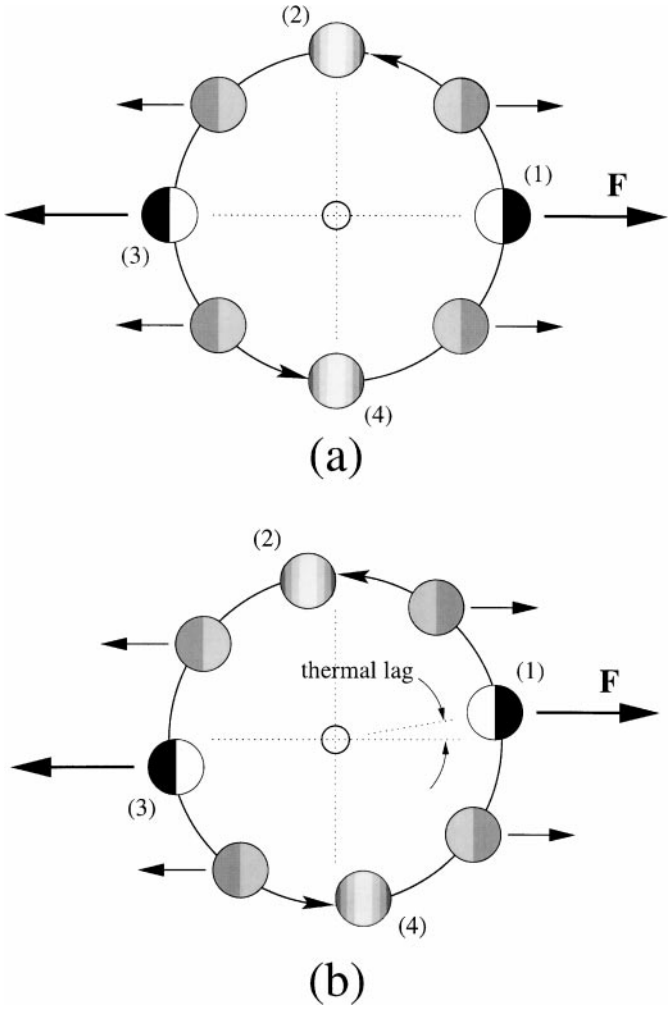

FIG. 2. A body on a circular orbit with its rotation axis in the orbital plane. (a) Without the seasonal lag, the situation is symmetric, so instantaneous changes in a caused by transverse force components cancel out over a complete orbit, resulting in no net change in a. (b) With seasonal lag, the symmetry is broken, causing net semimajor axis decay.

that the rate of semimajor axis decay does not depend on e. He also found that e always decreases and that the orientation of the semimajor axis, ϖ, always regresses. Orbits with larger eccentricities were beyond the scope and validity of Rubincam's approach.

In the general case, the Yarkovsky effect contains both diurnal and seasonal contributions, but its evaluation is not simply a matter of linearly combining separately calculated effects (we test such a procedure in this paper). The seasonal and diurnal effects are not components to be combined, but rather each represents the total Yarkovsky effect evaluated under a particular set of extreme parameters (diurnal: obliquity $= 0$ or π; seasonal: rotation period $= 0$). In this paper, we directly compute the changes in orbital elements caused by the *general* Yarkovsky effect, by which we mean any case that is neither purely seasonal nor purely diurnal.

3. NUMERICAL METHOD

To determine the thermal state of an asteroid, the heat equation is solved using a finite-difference scheme. A body is divided into discrete cells, throughout each of which the material properties and temperature are assumed to be uniform. The solar insolation boundary condition is computed at each timestep using an orbital integrator.

The mesh geometry is shown in Fig. 3a. In this paper, the body is assumed to be spherical, but the approach may be readily adapted to ellipsoidal bodies. The center of the body is occupied by a single spherical cell. Outside the central cell, the cell spacing is uniform in longitude and latitude. In the radial direction, cells are very thin near the surface in order to adequately resolve the temperature profile.

A typical noncentral cell is illustrated in Fig. 3b. $\hat{\mathbf{s}}_{ij}$ denotes the surface unit normal to each cell face. The first subscript refers to the spherical coordinate that is constant on the cell face and the second subscript ($j = +$ or $-$) distinguishes between the two faces which bound the cell in that direction. For example, $\hat{\mathbf{s}}_{r+}$ is the normal to the surface of a cell nearest the surface of the body. The central cell is bounded only in the radial direction, of course.

The temperature, T, in each cell of the body at time $t_0 + \Delta t$ is computed from the temperature at time t_0 in timesteps Δt using a first-order Euler scheme:

$$T(t_0 + \Delta t) = T(t_0) + \Delta t \left.\frac{\partial T}{\partial t}\right|_{t_0} + O(\Delta t^2). \qquad (1)$$

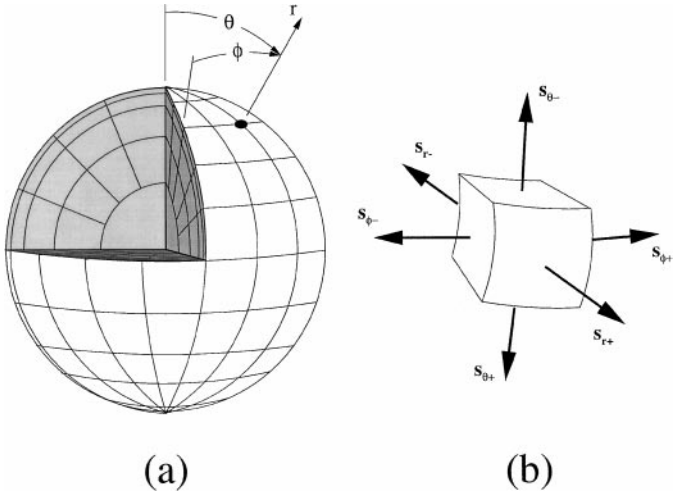

FIG. 3. (a) Schematic of the mesh used to solve the heat equation throughout the spherical body. Cells are uniformly spaced in longitude, ϕ, and latitude, θ. In the radial direction, the spacing varies, becoming very small at the surface. The center of the body is occupied by a single spherical cell. (b) Geometry of a typical (noncentral) cell. The normal vector for each face is identified by two subscripts. The first specifies which spherical coordinate (r, θ, or ϕ) is constant on the face. The second distinguishes between the two faces that bound the cell in that direction.

The size of Δt is limited by the smallest cell dimension in the mesh, because in a given time interval a thermal perturbation propagates a distance

$$l \sim \sqrt{\frac{k\Delta t}{\rho c_{\rm p}}}, \tag{2}$$

where k is the thermal conductivity, ρ is the density, and $c_{\rm p}$ is the heat capacity. If the timestep were so large that l exceeded the cell size, the integration would become unrealistic because cells communicate only with their immediate neighbors. This effect could be alleviated somewhat by using a higher-order scheme to evaluate spatial derivatives. Instead, we simply limited the timestep to be short enough (less than 100 s) to avoid this problem. A second-order scheme was tested and, to several significant figures, the results were found to be identical to those of the first-order scheme for the timestep we used.

The heat equation follows from conservation of energy. In a cell of volume V, the change in internal energy must equal the total heat flow through the cell boundary, yielding a formula for the temperature derivative $\partial T/\partial t$ in (1),

$$\rho V c_{\rm p} \frac{\partial T}{\partial t} = \oint \mathbf{J}(t) \cdot d\mathbf{s}, \tag{3}$$

where the integral is evaluated over the surface of each cell, $\mathbf{J}$ is the heat flux, and $d\mathbf{s}$ is the vector element of surface area. We assume that the cell size is small enough that the heat flux can be approximated as uniform over a given face, such that the total heat flow is calculated as

$$\begin{aligned}\oint \mathbf{J}(t_0) \cdot d\mathbf{s} = {} & J_{r+}A_{r+} + J_{r-}A_{r-} + J_{\theta+}A_{\theta+} \\ & + J_{\theta-}A_{\theta-} + J_{\phi+}A_{\phi+} + J_{\phi-}A_{\phi-},\end{aligned} \tag{4}$$

where A_{ij} and J_{ij} are the area and the heat flux on face (i, j), respectively. For any interior cell face, not exposed to the surface of the asteroid, the heat flux is conductive, so

$$J_{ij} = k(\nabla T)_{ij} \cdot \hat{\mathbf{s}}_{ij}. \tag{5}$$

The temperature gradient, $(\nabla T)_{ij}$, across face (i, j) of a cell centered at coordinates (r, θ, ϕ) is computed using a difference approximation of the directional derivative of the temperature field in the direction normal to the face; for example,

$$(\nabla T)_{r+} = \frac{T(r + \Delta r, \theta, \phi) - T(r, \theta, \phi)}{\Delta r}. \tag{6}$$

For surface cell faces, the heat flux (J_{r+}) is the difference between solar insolation inward and thermal radiation outward,

$$J_{\rm surface} = (1 - A)S_{\odot}(\hat{\mathbf{n}} \cdot \hat{\mathbf{r}}) - \epsilon\sigma T^4, \tag{7}$$

where Λ is the bond albedo, $S_{\odot}$ is the solar flux impinging on the asteroid, $\hat{\mathbf{n}}$ is the surface unit normal vector, and $\hat{\mathbf{r}}$ is the unit position vector of the sun with respect to the body. Of course, on the night side, the solar insolation is zero, leaving only the last term.

After the thermal state of the body is evaluated for a given timestep, the net radiative reaction force, $\mathbf{F}$, is evaluated by summing the vector thermal radiation forces on each exterior surface element,

$$\mathbf{F} = \sum_{i=1}^{n} \mathbf{f}_i A_i, \tag{8}$$

where $\mathbf{f}_i$ is the force per unit area due to the emission of radiation from surface cell i. The forces due to incident and reflected sunlight are neglected because they are purely radial (with respect to the Sun) and have the same form as solar gravity, resulting only in a very slight modification to the heliocentric motion with no secular variations. We assume that the emitted radiation (from any surface element) follows Lambert's law, such that the power radiated into unit solid angle is

$$I(\zeta) = \beta \cos(\zeta), \tag{9}$$

where ζ is the zenith angle. β is a normalization factor such that

$$\int I(\zeta)\, d\Omega = \epsilon_i \sigma T_i^4 A_i, \tag{10}$$

where the integral is taken over the outward hemisphere, ϵ_i is the emissivity of the surface element, and σ is the Stefan–Boltzmann constant. Thus, the net Yarkovsky force becomes

$$\mathbf{F} = \sum_{i=1}^{n} \frac{2}{3} \frac{\epsilon_i \sigma T_i^4}{c} \hat{\mathbf{n}}_i A_i. \tag{11}$$

The rates of change of the orbital elements are computed at each timestep by decomposing the Yarkovsky force vector and using the Gaussian form of the perturbation equations (Danby 1992). To obtain the net orbital element time derivatives, the perturbations are averaged over a single orbit (while the orbital elements are held constant).

In order for our calculations to be meaningful, the results must be independent of the timestep and the cell size. Based on initial experiments, we selected the largest Δt and cell size that appeared to reasonably satisfy this requirement. About 5% of the cases evaluated were selected at random and recomputed using approximately twice the number of cells and a very short timestep (10 s). In most cases, the high- and low-resolution results differ by less than 5%. In one case, the difference is about 9% (see Fig. 8).

Our results are useful only if the body is in a steady state such that the thermal state of the body, and hence the net Yarkovsky force vector, is a periodic function of the true anomaly. In order to achieve this thermal condition, the simulation must run during an

adequate warmup period. Based on experiments, we found that a single orbit was sufficient to warm up our calculation when the body's initial temperature was uniform at the appropriate effective temperature. About 5% of the cases were chosen at random and recomputed using a warmup period of two orbits. In all cases, the long- and short-warmup results differ by 1% or less.

A limiting problem with our simple calculation is that for very fast rotation, an impractically short timestep is required in order to adequately sample a single rotation. Periods of 1 h or less require a reduction in timestep, which makes a broad exploration of the parameter space impractical with the available computing resources. According to Harris (1979), typical rotation periods for well-consolidated, stony bodies with sizes of 1, 10, and 100 m may be around a minute, several minutes, and a few hours, respectively. Farinella *et al.* (1998) suggest even shorter periods. Observations of bodies with diameters of tens of meters also suggest much shorter rotation periods (Pravec *et al.* 2000). Thus, even for the largest bodies in this study, it is probably not practical to simulate realistic rotation rates using our current method. However, although the results for finite rotation rate can differ substantially from those for which fast rotation is assumed to hold, in many cases of interest, there is a fast rotation regime, in which the results are insensitive to the rotation rate. In the future, additional cases with more realistic rotation rates can be explored by modifying our scheme such that full rotation periods are sampled at intervals around an orbit, assuming that the thermal state of the asteroid varies sufficiently gradually.

4. RESULTS

In this section, we present our results for the rates of change of semimajor axis caused by the general Yarkovsky effect. First, we compare our calculations with those of previous workers by attempting to simulate some simple cases that they have evaluated, specifically the pure seasonal or diurnal cases. Then we extend those simulations to orbits with higher eccentricity and bodies with intermediate obliquity for which we observe behavior that is beyond the scope of the previous theory.

4.1. Pure Diurnal Effect, Circular Orbit

Peterson (1976) presented an analytical theory of the pure diurnal ($\iota = 0$ or π) Yarkovsky effect in which the Fourier expansion of the surface temperature distribution is truncated to third order. He presented results for a 1-m body spinning with a 5-h period. In Fig. 4, we compare our calculations with Peterson's analytical results for that case. Our parameters are exactly analogous to Peterson's. The properties of the body are identical to those used by Peterson for stony material: $\rho = 2500$ kg m^{-3}, $k = 1.5$ W m^{-1} K^{-1}, $c_p = 1000$ J kg^{-1} K^{-1}, $\epsilon = 1$, $\Lambda = 0$. We find that our calculation produces semimajor axis decay that is systematically slower than Peterson's by about 10%, but that the overall trend is in reasonable agreement for this case, in which his assumptions are applicable.

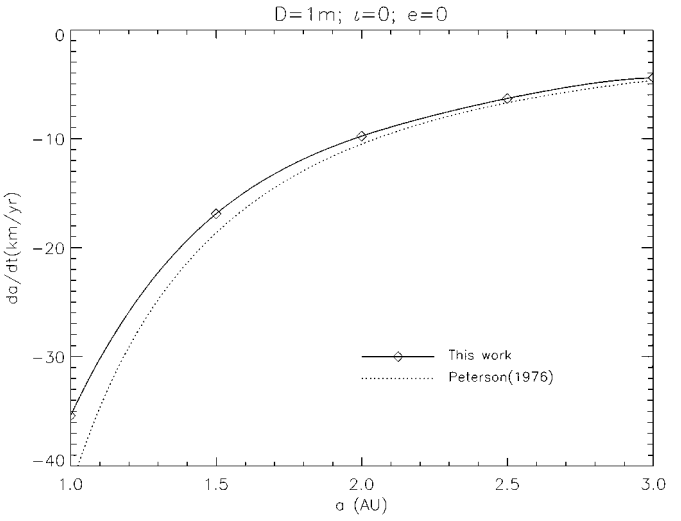

FIG. 4. Comparison between our results and those of Peterson (1976) for da/dt for a 1-m stony body with a 5-h rotation period for the case $\iota = \pi$, resulting in a pure diurnal Yarkovsky effect. Diamonds indicate our computational results, interpolated by the solid lines. The dotted curve is Peterson's result.

4.2. Pure Seasonal Effect, Circular Orbit

The pure seasonal Yarkovsky effect was evaluated analytically by Rubincam (1995, 1998) by linearizing the radiative term in the boundary condition. Rubincam pointed out that his approach leads to an underestimate of the surface temperature asymmetry and an overestimate of the thermal lag angle, so he applied an estimated correction factor of 0.75 to da/dt in order to correct for these effects. We have used our numerical method to calculate da/dt for the case evaluated by Rubincam. We studied bodies with the same physical properties used by Rubincam (1998) for stony material: $\rho = 3500$ kg m^{-3}, $k = 2.4$ W m^{-1} K^{-1}, $c_p = 750$ J kg^{-1} K^{-1}, $\epsilon = 1$, $\Lambda = 0$. However, while Rubincam assumed infinitely fast rotation (in order to eliminate diurnal effects and show the pure seasonal effect), we are restricted to a finite rotation rate.

We compared results for the case $\iota = \pi/2$, $e = 0$, $D = 20$ m, using various rotation periods in our calculation. As shown in Fig. 5, we find that within the range for a used here, our results are independent of rotation rate at all a values of interest for rotation periods less than about a day. In such a fast rotation regime, our results differ from Rubincam's by about 5 to 10%, well within the expected margin of error for Rubincam's approach.

In Fig. 6, we compare our calculation to that of Rubincam (1998) for 1-, 10-, and 100-m bodies with $\iota = \pi/2$, $e = 0$, and $p = 5$ h. We find that our calculation produces semimajor axis decay that is faster than Rubincam's by 20–40% for the 1-m body and around 10% for the 10-m body. For the 100-m body, our calculation produces semimajor axis decay that is generally a few percent slower than Rubincam's, but the curves cross at about 0.6 AU. Based on a plane-parallel heat-flow approximation, Vokrouhlický and Farinella (1998) also reported that for 100-m bodies, Rubincam's formula yields faster semimajor axis

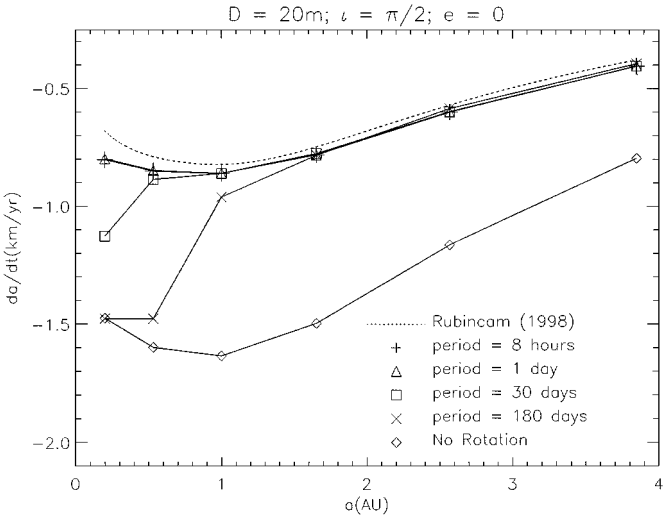

FIG. 5. Rate of change of a as a function of rotation period. We find that for periods of about a day or faster, da/dt does not depend on the rotation period, permitting a comparison between our finite rotation rate results and the infinite rotation rate (pure seasonal) results of Rubincam (1998). Symbols indicate our computed results, connected by solid lines. The dotted curve is Rubincam's result.

decay than their nonlinearized theory, and they confirmed that his theory tends to underestimate the surface temperature asymmetry and overestimate the thermal lag angle. In all cases, the trends are in agreement between our results and Rubincam's and the qualitative differences probably reflect the acknowledged approximations involved in Rubincam's analytical approach. The magnitude of the disagreement is not significant for application to solar system problems.

4.3. Pure Diurnal Effect, Noncircular Orbit

In this section, we investigate the pure diurnal effect ($\iota = 0$ or π) by varying the size, rotational sense (prograde/retrograde), semimajor axis, and eccentricity of test bodies rotating with a 5-h period, whose physical properties are the same as those in the previous section. Figure 7 summarizes the results for da/dt for this wide range of cases.

Note in Fig. 7 that, for large values of e, da/dt is quite large, and a steep function of e. For example, for any size body, at 1 AU, the semimajor axis of an orbit with $e = 0.9$ evolves about 10 times more rapidly than for a nearly circular ($e = 0.1$) orbit, while at 3 AU this factor is closer to 50. The faster orbital evolution is probably the result of the stronger force that the body experiences near pericenter, relative to the circular orbit. This effect competes with, but dominates, the fact that most of the orbital period is spent at heliocentric distances larger than a, where the force is weaker relative to the circular orbit.

This observation can be supported heuristically (at least for moderate eccentricities) by considering Peterson's form for the diurnal Yarkovsky force as a function of heliocentric distance (Peterson 1976), which can be written

$$F(r) \simeq \psi \left(\frac{r}{a}\right)^{-7/2}, \tag{12}$$

where ψ does not depend on r. This result was based on the assumption that the temperature distribution throughout the body at any heliocentric distance is that obtained in a body on a circular orbit of radius r. Actually, for a noncircular orbit, the true temperature distribution contains transients which are not accounted for by this simplification, so this assumption is probably only useful for small or moderate eccentricities. If the rotation period is much shorter than the orbital period, then for this case ($\iota = 0$ or π), the thermal lag angle, δ, can be considered to be roughly independent of the true anomaly, allowing the Yarkovsky force (12) to be decomposed (into radial and transverse components) as

$$\begin{aligned} R(r) &\simeq \psi \cos\delta \left(\frac{r}{a}\right)^{-7/2} \\ B(r) &\simeq \psi \sin\delta \left(\frac{r}{a}\right)^{-7/2}. \end{aligned} \tag{13}$$

The semimajor axis changes at a rate (Danby 1992) of

$$\frac{da}{dt} = \frac{2}{n}\left[R(r)\frac{e}{\sqrt{1-e^2}}\sin f + B(r)\frac{a\sqrt{1-e^2}}{r}\right], \tag{14}$$

where n is the mean motion and f is the true anomaly. Over an orbit, $R(r)\sin f$ averages to zero for any eccentricity and $|\langle B(r)/r\rangle|$ can be shown to increase monotonically at an increasing rate with e (see Appendix). From (14),

$$\left|\left\langle\frac{da}{dt}\right\rangle\right| = \frac{2a}{n}\sqrt{1-e^2}\left|\left\langle\frac{B(r)}{r}\right\rangle\right|. \tag{15}$$

For moderate e, this function increases monotonically with e in a manner qualitatively similar to the observed e-dependence in Fig. 7. If the r-dependence in Eq. (12) were considerably weaker ($F(r) \propto (r/a)^{-1/2}$, for example), then the increased force near periapse would not be strong enough to cause a net increase in $|\langle da/dt\rangle|$ during the relatively short time spent at heliocentric distances smaller than a. In that case, $|\langle da/dt\rangle|$ would decrease with increasing e. For larger e, this heuristic analysis is inadequate.

Other features of Fig. 7 can be interpreted physically:

(1) When the body's rotation is reversed, da/dt has nearly identical values except that the sign is reversed. This near-antisymmetry exists because, for prograde/retrograde rotation, the angular motion of the sun in the sky, as seen from a fixed point on the surface of the body, is the sum/difference of the body rotation rate and the orbital rotation rate. Since the rotation period is much shorter than the orbital period (except near periapse on

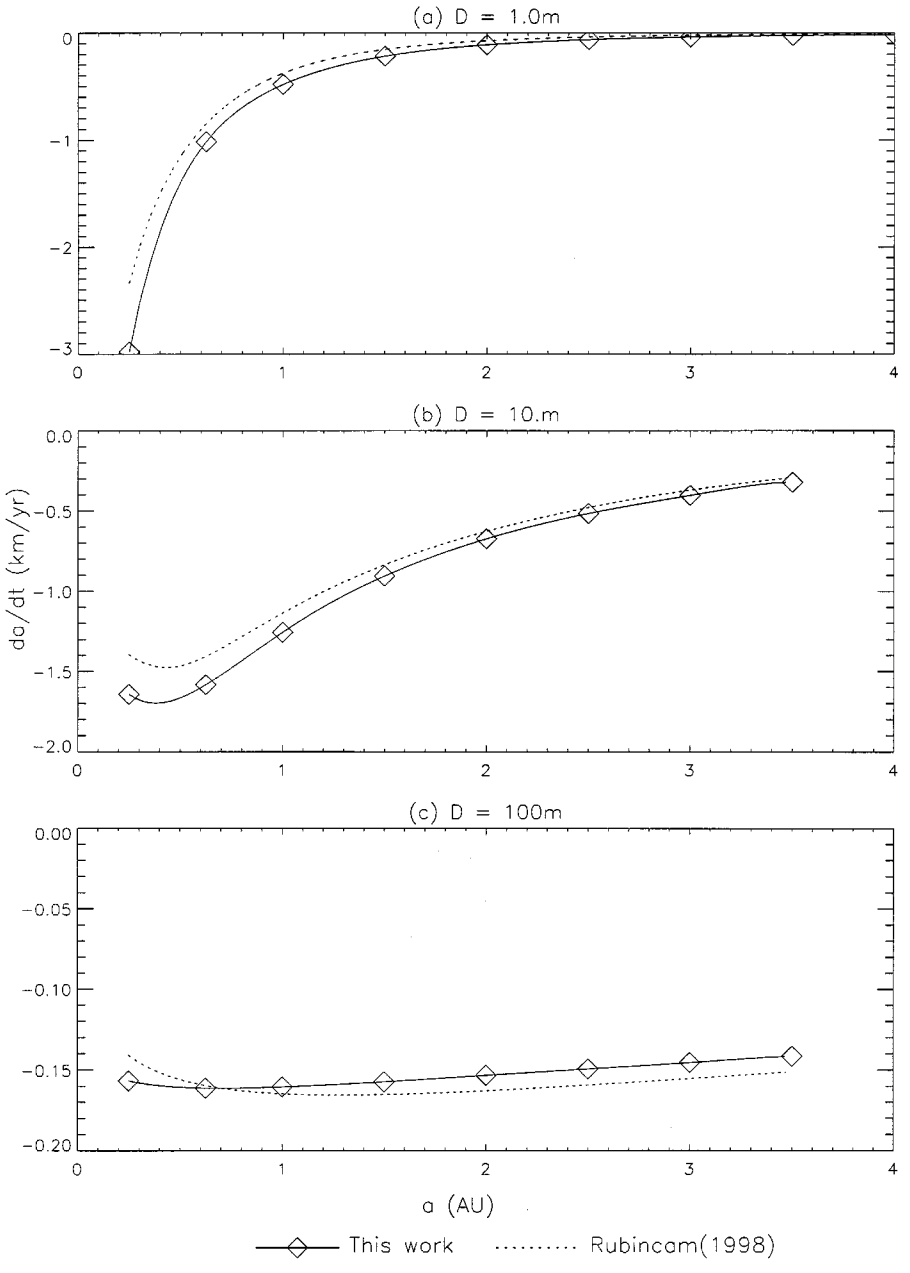

FIG. 6. Comparison between our finite-rotation rate (period = 5 h) results and the infinite rotation rate (pure seasonal) results of Rubincam (1998) for da/dt for 1-, 10-, and 100-m stony bodies for the case $\iota = \pi/2$. Diamonds indicate our computational results, interpolated by the solid lines. The dotted curve is Rubincam's result.

high eccentricity orbits), the acceleration vectors for each case should nearly be reflections of one another about the radial line.

(2) For fixed e, a, and ι, da/dt roughly scales inversely with the radius of the body. This behavior is consistent with all of the test bodies being in the same thermal regime (corresponding to the plane-parallel approximation). In this case, the rotation is fast enough that even the smallest body is affected only in a relatively thin surface layer. As a result, the surface temperature distribution, $T(\theta, \phi)$, is roughly the same for all sizes in the experiment. It is easy to show that, under this assumption, the Yarkovsky accelerations, and ultimately da/dt, must vary inversely with the radius of the body simply because of the size dependences of surface area and volume. Any deviation from this size dependence is a reflection of the slight size dependence of the surface temperature distribution.

4.4. Cases of the General Yarkovsky Effect: $e \neq 0$, $\iota = \pi/2$

In this section, we vary D, a, e, and α for test bodies with $\iota = \pi/2$, rotating with a 5-h period, whose properties are the same as those in the previous section. When e is small, we are

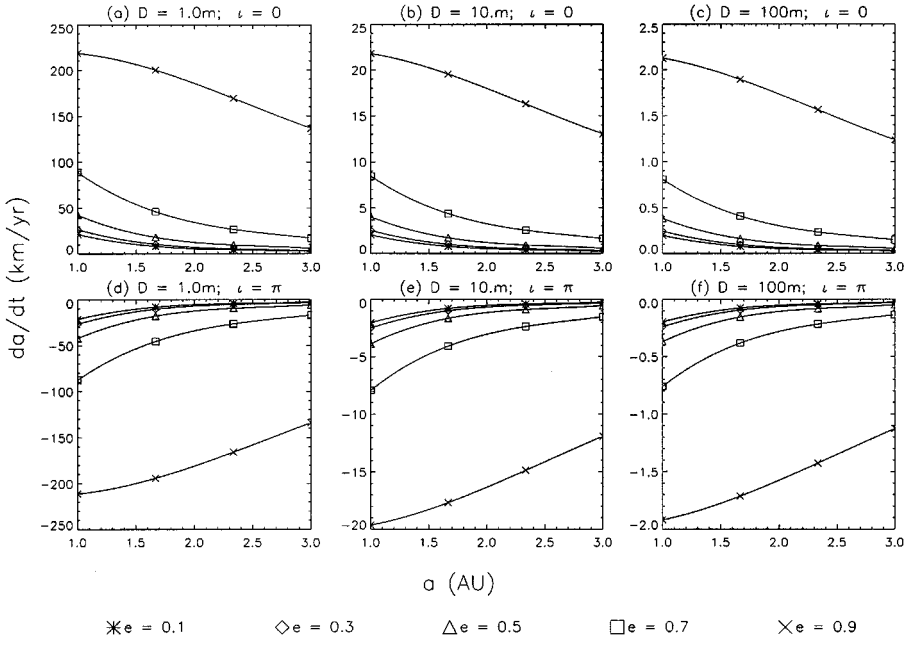

FIG. 7. da/dt vs a for $\iota = 0$ or π, $e = 0.1$–0.9, rotation period = 5 h. Symbols indicate our computed results; solid curves are interpolated. This configuration gives rise to the pure "diurnal" Yarkovsky effect. As expected, the da/dt curves for retrograde rotation ($\iota = \pi$) are nearly identical to those for prograde rotation ($\iota = 0$) except for a change in sign. The $1/R$ dependence of da/dt is obvious. Also, da/dt is quite large for orbits with large e.

essentially reproducing the pure seasonal effect. However, for orbits with higher eccentricity, we observe more general effects which are not necessarily due to purely seasonal forcing, because we use a finite rotation rate. Figure 8 summarizes the results for da/dt. Four orientations for $\alpha - 0, \pi/4, \pi/2, 3\pi/4-$ were investigated. Four other orientations correspond to reversing the rotation rates and it is expected that the results will be identical except that the inclination changes, which are caused by the diurnal forcing (and not presented in this paper), will be opposite.

A number of interesting features in Fig. 8 call for some discussion:

(1) In plots (j), (k), and (l) of Fig. 8, da/dt changes sign, becoming large and positive for orbits with large e and small a. This behavior is associated with the finite (as opposed to infinite) rotation rate used in our calculation. Near periapse, the angular motion of the sun in the sky becomes comparable to the rotation rate. Relative to the infinitely fast rotation case, the incident energy is redistributed such that, instead of being spread uniformly over lines of constant latitude, it is concentrated somewhat on the day side. This hot spot causes the force vectors to be more radial near periapse. Very close to periapse, this reduces whatever prograde or retrograde components may be present. Further from periapse, force vectors become more retrograde as the body approaches periapse and more prograde as the body recedes from periapse. The net effect on da/dt depends on a and e in a complicated way, but for this case, in which $\alpha = 3\pi/4$, the strongest retrograde components should occur near periapse (for infinitely fast rotation), but they are reduced by the effect of the hot spot, allowing prograde forces from other parts of the orbit to dominate the semimajor axis evolution. Note that the magnitude of this effect should depend strongly on the rotation rate of the body. An analogous effect is seen in the $\alpha = \pi/4$ case (plots (d), (e), and (f) of Fig. 8).

(2) In plots (b) and (c) of Fig. 8, $|da/dt|$ begins to decrease at small a for orbits with large e. The behavior is most pronounced for the 100-m body and not apparent for the 1-m body. This result can be explained as follows.

First, consider a circular orbit (e.g., Fig. 6b). The polar temperatures for a body on such an orbit with $\iota = \pi/2$ oscillate seasonally, reaching maximum values (hottest anywhere on the body ever) and minimum (coldest anywhere on the body ever) twice every orbit (near the times when the rotation axis points directly toward or away from the sun). This temperature variation launches seasonal heat pulses into the body. For this $e = 0$ case, one can think of two identical heat pulses with opposite phases, centered near the poles. The magnitude and direction of the Yarkovsky force can be related to the timing of the pulses. For orbits with small a, and hence short orbital periods, the heat pulses do not penetrate deeply, so smaller a (shorter orbital period) leads to a smaller net Yarkovsky force and hence smaller $|da/dt|$. For larger a and hence longer orbital periods, the heat pulses affect the entire body, producing a larger net Yarkovsky force whose magnitude does not depend strongly on a. Moreover, for a given thermal inertia, the thermal lag angle increases as the orbital period is shortened, favoring an increase in $|da/dt|$ as a is decreased and more of the Yarkovsky force is directed along the orbital track. Finally, since the solar heating decreases with a, there is a tendency for the magnitude of the force also to be smaller with increasing a.

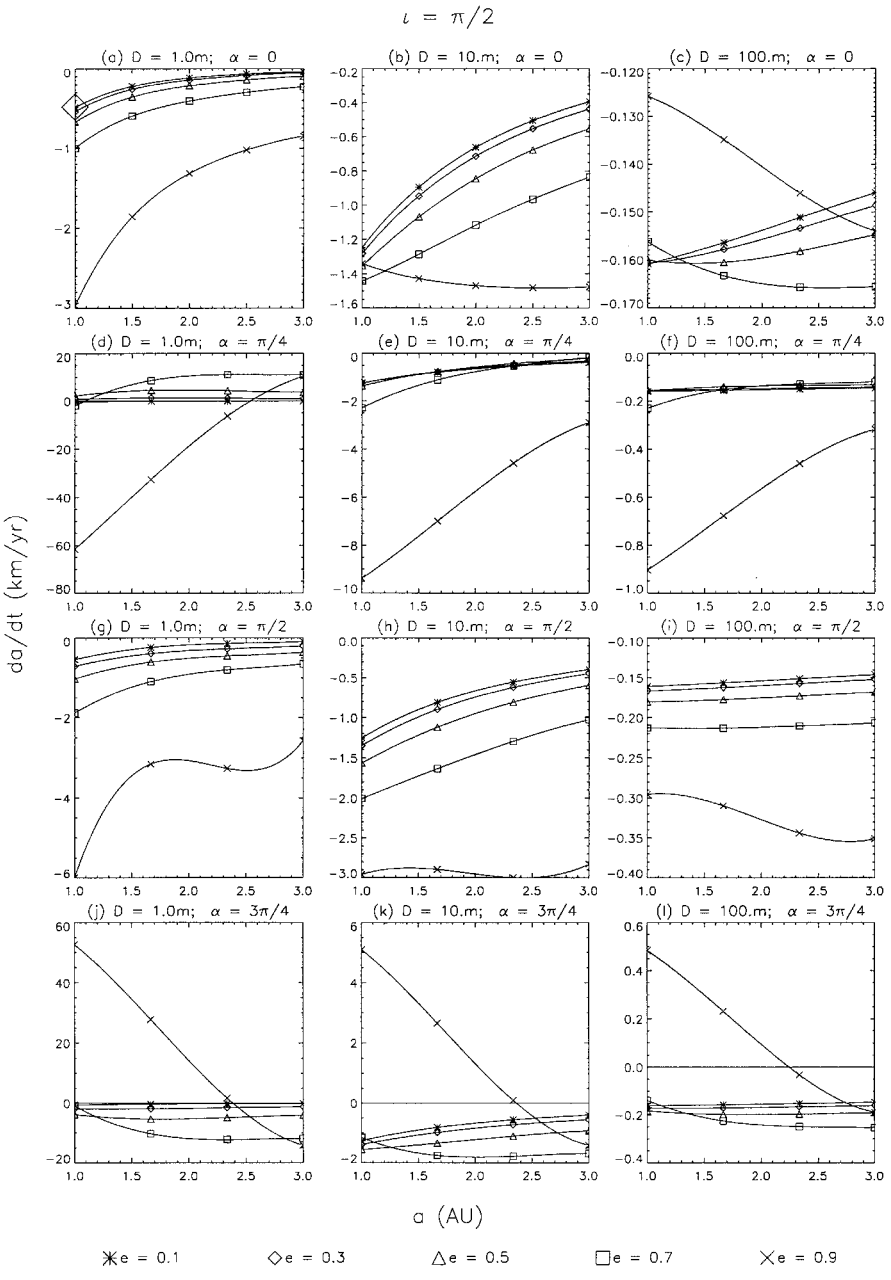

FIG. 8. da/dt vs a for $\iota = \pi/2$, $e = 0.1$–0.9, rotation period = 5 h. Symbols indicate our computed results; solid curves are interpolated. For small e, this configuration essentially yields the pure "seasonal" Yarkovsky effect. However, because the rotation rate is not infinite, the effect is more complicated for larger e. The point in (a) highlighted with a large diamond produced a 9% discrepancy when recomputed using a higher resolution and shorter timestep. This example is the largest discrepancy found in this work.

Now consider what happens for larger e (with $\alpha = 0$). As e is increased, one seasonal heat pulse becomes stronger and the other becomes weaker. Furthermore, the strong pulse becomes narrower (i.e., it becomes more concentrated around periapse) and the weak pulse becomes wider. For a given a, e can be increased to such a value that, although the body at this a with $e = 0$ would have a large Yarkovsky force vector because it is completely affected by the seasonal heat pulse, the strong heat pulse is too short to significantly penetrate the body, so the magnitude of the force decreases. In other words, for a given a at which the body is penetrated by the $e = 0$ seasonal heat pulses, a value of e exists above which the strong solar heating at periapse only affects a surface layer. This threshold value of e should increase with a and decrease with the size of the body, consistent with the trends in the figure.

(3) We are unable to offer a specific explanation for the curious behavior (non-monotonic dependence of da/dt on a) in plots (g), (h), and (i) of Fig. 8, but given the various effects which

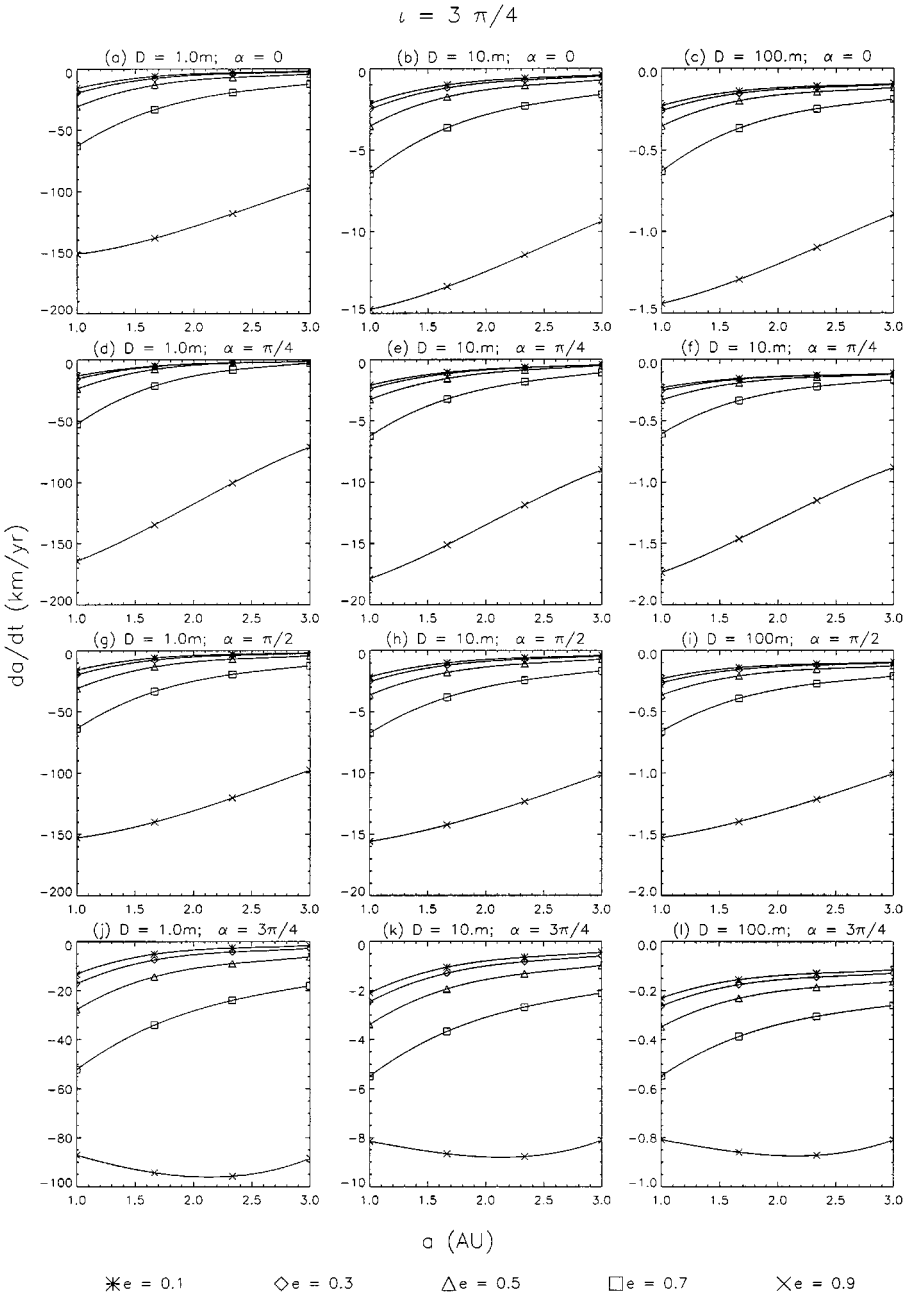

FIG. 9. da/dt vs a for $\iota = 3\pi/4$, $e = 0.1$–0.9, rotation period = 5 h. Symbols indicate our computed results; solid curves are interpolated. This configuration corresponds to neither the pure "diurnal" nor the pure "seasonal" approximation, but the results are roughly consistent with a suitable linear combination of our $\iota = 0$ or π and $\iota = \pi/2$ results from previous figures (see Fig. 10).

contribute to the semimajor axis evolution in a complicated way, it is not surprising that they would conspire to produce the observed trends.

4.5. *Cases of the General Yarkovsky Effect: $e \neq 0$, $\iota = 3\pi/4$*

In the previous section, it was seen that, for $\iota = \pi/2$, our finite rotation rate produced effects which are more general than those produced in the case of infinitely fast rotation. In this section we look at cases with finite rotation rate ($p = 5$ h) and an intermediate obliquity ($\iota = 3\pi/4$). The body properties are the same as in the previous sections. Figure 9 summarizes the results for da/dt. Four orientations for α $(0, \pi/4, \pi/2, 3\pi/4)$ were investigated. The other orientations, α, and opposite obliquity ($\iota = \pi/4$) were not investigated, but are expected to give qualitatively similar results (with a change of sign for the opposite obliquity cases).

The results in Fig. 9 are roughly consistent with what one would obtain from a linear combination of our results for the

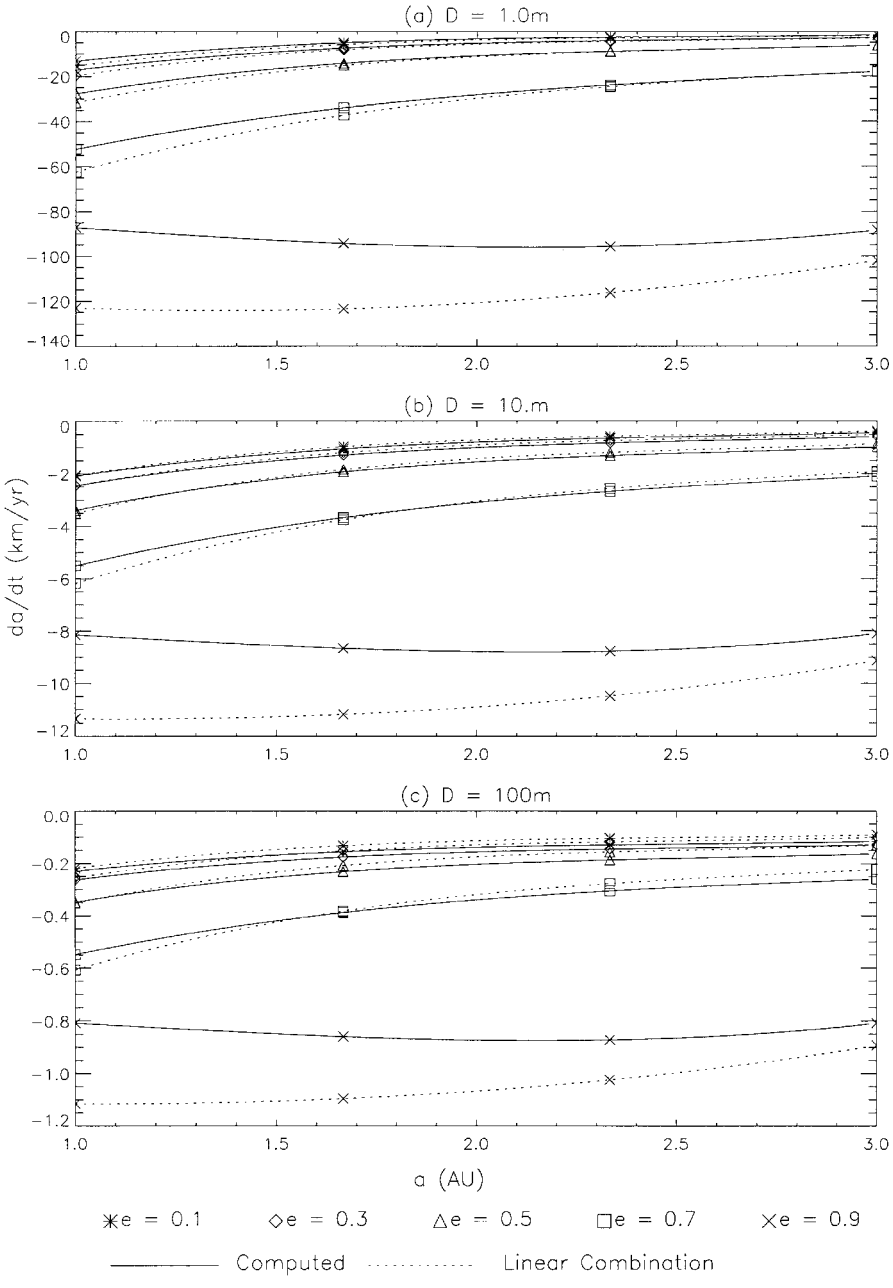

FIG. 10. The linear superposition of "diurnal" and "seasonal" endmember components can approximate the results of our general calculations. For a range of body sizes (D), semimajor axes (a), and eccentricities (e), we show the results of our general calculations (solid curves) compared with results obtained using Eq. (16) (dotted curves), where we combine our diurnal approximation (Figs. 7d, 7e, and 7f; $\iota = \pi$) with our seasonal approximation (Figs. 8j, 8k, and 8i; $\iota = \pi/2, \alpha = 3\pi/4$). Symbols indicate computed results; curves are interpolated. Agreement is close for smaller bodies with larger a and smaller e. The superposition approximation is worst for cases of large e and small a because temperature excursions in the body are the most severe for those cases.

pure diurnal and pure seasonal extremes (from Sections 4.3 and 4.4, respectively) using coefficients that are consistent with the theories of Öpik (1951) and Rubincam (1987); i.e.,

$$\frac{da}{dt} = \cos\iota \left.\frac{da}{dt}\right|_{\text{diurnal}} + \sin^2\iota \left.\frac{da}{dt}\right|_{\text{seasonal}}. \qquad (16)$$

Such a linear superposition is not strictly valid, however, because the radiative term in the boundary condition makes the problem nonlinear. The nonlinear effects become significant for cases where temperature excursions in the body are large. That condition occurs for highly noncircular orbits and slowly rotating bodies. To demonstrate that effect, in Fig. 10 we show a comparison between our direct general calculations and the linear superposition (Eq. (16)) where the diurnal contribution is from Figs. 7d, 7e, and 7f and the seasonal contribution is from

Figs. 8j, 8k, and 8l. As expected, the linear combination works well for small e, where temperature excursions are small, but not as well for larger e and small a, where temperature excursions are large.

5. DISCUSSION

We have presented a fully numerical, three-dimensional solution to the heat equation for an orbiting body in the solar radiation field that allows us to investigate the general Yarkovsky effect for regions of parameter space that have not been accessible to previous methods. Our calculations have been validated against those of previous workers where results are available for comparison. We have validated our calculation with respect to timestep, spatial resolution, and warmup period. We find that the results presented in this paper should be reliable to within about 5% or better. One resolution validation run produced an error or about 9% and is emphasized in Fig. 8a.

Using our numerical approach, we have conducted a fairly coarse survey of a parameter space consisting of semimajor axis, eccentricity, spin axis direction, and size. da/dt is the strongest effect, but de/dt and di/dt can also be fairly strong. $d\varpi/dt$ is a smaller effect, which may be important only on timescales longer than that for collisional reorientation of the spin vector. In this paper, we have presented the results for da/dt. A subsequent paper will focus on changes in other orbital elements.

The results in Fig. 9 demonstrate that, for high-eccentricity orbits, the Yarkovsky effect can produce very rapid changes in a. For example, in Fig. 9, da/dt for a 1-m stony body with $a = 2.5$ and $e = 0.9$ corresponds to a rate of 1 AU in about 1.5 My. Given the uncertainties in thermal properties, it is plausible that the semimajor axis could change as fast as 1 AU or more per million years for stony bodies with diameters of 1 m or so. It also appears that the rates could be substantially faster if e were increased beyond 0.9. This region of parameter space is relevant to the fate of small stony bodies trapped in the strong main-belt resonances. In the absence of the Yarkovsky effect, these bodies have been shown to undergo rapid changes in e, approaching 1, causing most to become either sun-grazers or Jupiter-crossers on timescales of several millions of years (Farinella *et al.* 1994, Gladman *et al.* 1997). Our results suggest that there may be a role for the Yarkovsky effect in the orbital evolution of these bodies once their eccentricities become large. In 10^5 years, the Yarkovsky effect alone might be able to change the semimajor axis of a small stony body by as much as 0.1 AU, comparable to the width of the 3:1 resonance, for example. Changes in other orbital elements may also be important.

A major problem with applying this idea to the solar system is that the rates of semimajor axis evolution presented in this paper are based on rotation rates that seem implausibly slow to be typical of such small bodies (see Section 3). The large values of $|da/dt|$ in Fig. 9 contain a substantial diurnal component which should be much smaller (essentially absent) for bodies rotating with more plausible periods of say, 1 min or less. On the other hand, (Rubincam 2000) suggests a Yarkovsky-like mechanism (the YORP effect) for slowing asteroid rotation rates. However, slow rotators of this size (1 m or so) may not be in a state of principal axis rotation. The Yarkovsky effect has yet to be investigated under such a condition.

The question of whether the Yarkovsky effect can be strong enough to be important in the orbital evolution of small bodies in the strong main-belt resonances requires a study of the orbital evolution of small bodies subject to the simultaneous influence of the Yarkovsky effect and these resonances. This study will be the topic of a future paper.

In the current study, we considered only homogeneous bodies and assumed that the dependence of thermal diffusivity on temperature is not important. These assumptions may be valid for small (1- to 10-m) bodies, but larger bodies are likely to possess a regolith and possibly even a porous interior. Some work has already been done on nonhomogeneous bodies. Assuming a temperature-independent thermal diffusivity, Vokrouhlický and Brož (1999) looked at models possessing an insulating surface layer and found a significantly increased semimajor-axis mobility for fragments of 10 m and larger and a significantly decreased mobility for meter-sized fragments. Our code is designed to handle a more realistic calculation of the Yarkovsky effect on inhomogeneous bodies, in which two or more layers with differing thermal properties and a temperature-dependent thermal diffusivity are treated. Similarly, although we treated spherical bodies in this study, in principle our approach is applicable to nonspherical bodies, as long as their shapes are such that no shadows are cast. Such a treatment would require moderate modifications to our code. We intend to perform such calculations in the near future.

The power of our numerical approach having been demonstrated and its validity confirmed by agreement with previous studies in the limited cases where those methods apply, our future work will address nonspherical bodies and a range of thermal properties, including more realistic thermal diffusivities. Under special circumstances, the Yarkovsky effect has been shown to be stronger than had been previously demonstrated. Extended studies may reveal additional circumstances under which the Yarkovsky effect is strong enough to play a role in the transport of small bodies in the solar system.

APPENDIX

Here we show that, as claimed in Section 4.3, $|\langle B(r)/r\rangle|$ increases monotonically with e and increases more quickly with increasing e. Since $r/a = (1 - e\cos E)$, the average of $B(r)/r$ over an orbit is given by

$$\left\langle \frac{B(r)}{r} \right\rangle = \frac{\psi \sin\delta}{2\pi a} \int_0^{2\pi} (1 - e\cos E)^{-7/2}\, dE, \tag{17}$$

where E is the eccentric anomaly. Now $(1 - e\cos E)^{7/2}$ can be expanded in a Taylor series about $e = 0$:

$$(1 - e\cos E)^{-7/2} = 1 + \frac{7}{2} e\cos E + \frac{63}{8} e^2 \cos^2 E + O(e^3). \tag{18}$$

Equation (18) is an infinite series in powers of $e \cos E$ in which all of the coefficients are positive. Substituting (18) into (17) and integrating, we obtain

$$\left\langle \frac{B(r)}{r} \right\rangle = \frac{\psi \sin\delta}{2\pi a}\left[2\pi + \frac{7}{2}e\int_0^{2\pi} \cos E\, dE + \frac{63}{8}e^2\int_0^{2\pi} \cos^2 E\, dE + O(e^3)\right]. \quad (19)$$

Since all of the coefficients in (19) are positive and

$$\int_0^{2\pi} \cos^n E\, dE = \begin{cases} 0 & : n \text{ odd} \\ \text{a positive number} & : n \text{ even}, \end{cases} \quad (20)$$

$|\langle B(r)/r\rangle|$ is a monotonically increasing function of e. As e is increased, higher powers of e become significant and since their coefficients are all positive, $|\langle B(r)/r\rangle|$ increases more rapidly with increasing e (this observation is confirmed by taking the second derivative of (19) with respect to e).

ACKNOWLEDGMENTS

We acknowledge D. Vokrouhlický and D. P. Rubincam for their helpful reviews. We also thank W. F. Bottke for helpful discussions and P. Downey for providing additional computing resources. This work was supported under Grant NAG5-3631 from the NASA Planetary Geology and Geophysics Program.

REFERENCES

Afonso, G. B., R. S. Gomes, and M. A. Florczak 1995. Asteroid fragments in Earth-crossing orbits. *Planet. Space Sci*. **43**, 787–795.

Danby, J. M. A. 1992. *Fundamentals of Celestial Mechanics*. William–Bell, Richmond.

Farinella, P., and D. Vokrouhlický 1999. Semimajor axis mobility of asteroidal fragments. *Science* **283**, 1507–1510.

Farinella, P., R. Froeschlé, Ch. Froeschlé, R. Gonzi,G. Hahn, A. Morbidelli, and G. B. Valsecchi 1994. Asteroids falling into the Sun. *Nature* **371**, 314–315.

Farinella, P., D. Vokrouhlický, and W. K. Hartmann 1998. Meteorite delivery via Yarkovsky orbital drift. *Icarus* **132**, 378–387.

Gladman, B. J., F. Migliorini, A. Morbidelli, V. Zappala, P. Michel, A. Cellino, C. Froeschlé, H. F. Levison, M. Bailey, and M. Duncan 1997. Dynamical lifetimes of objects injected into asteroid belt resonances. *Science* **277**, 197–201.

Halliday, I., A. A. Griffin, and A. T. Blackwell 1996. Detailed data for 259 fireballs from the Canadian camera network and inferences concerning the influx of large meteorites.*Meteorit. Planet. Sci*. **31**, 185–217.

Harris, A. W. 1979. Asteroid rotation rates. II. A theory for the collisional evolution of rotation rates. *Icarus* **40**, 145–153.

Öpik, E. J. 1951. Collision probabilities with the planets and the distribution of interplanetary matter. *Proc. R. Irish Acad*. **54**, 165–199.

Peterson, C. 1976. A source mechanism for meteorites controlled by the Yarkovsky effect. *Icarus* **29**, 91–111.

Pravec, P., C. Hergenrother, R. Whitely, L. Sarounová, P. Kusnirák, and M. Wolf 2000. Fast rotating asteroids 1999 TY2, 1999 SF10, and 1998 WB2. *Icarus*, submitted for publication.

Radzievskii, V. V. 1952. A mechanism for the disintegration of asteroids and meteorites. *Astron. Zh.* **29**, 162–170.

Rubincam, D. P. 1987. LAGEOS orbit decay due to infrared radiation from Earth. *J. Geophys. Res*. **92**, 1287–1294.

Rubincam, D. P. 1988. Yarkovsky thermal drag on LAGEOS. *J. Geophys. Res*. **93**, 13805–13810.

Rubincam, D. P. 1995. Asteroid orbit evolution due to thermal drag. *J. Geophys. Res*. **100** (E1), 1585–1594.

Rubincam, D. P. 1998. Yarkovsky thermal drag on small asteroids and Mars–Earth delivery. *J. Geophys. Res*. **103** (E1), 1725–1732.

Rubincam, D. P. 2000. Radiative spin-up and spin-down of small asteroids. *Icarus* **148**, 2–11.

Vokrouhlický, D., and M. Brož 1999. An improved model of the seasonal Yarkovsky force for regolith-covered asteroid fragments. *Astron. Astrophys*. **350**, 1079–1084.

Vokrouhlický, D., and P. Farinella 1998. The Yarkovsky seasonal effect on asteroidal fragments: A nonlinearized theory for the plane-parallel case. *Astron. J.* **116**, 2032–2041.

Vokrouhlický, D., and P. Farinella 1999. The Yarkovsky seasonal effect on asteroidal fragments: A nonlinearized theory for spherical bodies. *Astron. J*. **118**, 3049–3060.

Vokrouhlický, D., and P. Farinella 2000. Delivery of stony meteorites from the asteroid belt: A dynamical–collisional Monte Carlo model. *Nature*, submitted for publication.

Wetherill, G. W. 1985. Asteroidal source of ordinary chondrites. *Meteorit*. **20**, 1–22.

Wetherill, G. W. 1987. Dynamical relations between asteroids, meteorites, and Apollo–Amor objects. *Philos. Trans. R. Soc. London Ser. A* **323**, 323–337.

Wetherill, G. W., and D. O. ReVelle 1981. Which fireballs are meteorites—A study of the Prairie Network photographic meteor data. *Icarus* **48**, 308–328.